Temperature and Pressure Dependence Study of the Reaction of IO Radicals with Dimethyl Sulfide by Cavity Ring-Down Laser Spectroscopy

Yukio Nakano, Shinichi Enami, Shinji Nakamichi, Simone Aloisio,† Satoshi Hashimoto, and Masahiro Kawasaki*

Department of Molecular Engineering, Kyoto University, Kyoto 606-8501, Japan

Received: February 27, 2003; In Final Form: June 4, 2003

The reaction of IO radicals with dimethyl sulfide was studied using cavity ring-down laser spectroscopy. The reaction rate constant shows both a temperature and pressure dependence. At 100 Torr total pressure, the reaction has reached its high-pressure limit and has a rate constant of $(2.5 \pm 0.2) \times 10^{-13}$ molecule^{-1} cm^3 s^{-1} at 298 K. On the basis of the Arrhenius plot in the region of 273−312 K, the reaction has a negative activation energy ($E_a = -18.5 \pm 3.8$ kJ mol^{-1}). The atmospheric implications of these findings are discussed. In light of these new data, DMS oxidation by IO can compete with oxidation by the hydroxyl radical in the marine boundary layer. Quoted uncertainties are one standard deviation from regression analysis.

1. Introduction

The oxidation of dimethyl sulfide (DMS) is of particular importance to the production of atmospheric aerosols, especially in the marine boundary layer (MBL) because DMS is the main sulfur-containing species emitted from the oceans.[1] DMS is a relatively reduced form of sulfur and is produced biologically.[2] When oxidized, however, the organic sulfur species become hygroscopic and may form condensation nuclei, leading to the production of aerosols and possibly clouds.[3] The effects of aerosols and clouds remain as the largest uncertainty in climate forecasting today.[4] For this reason, the understanding of DMS oxidation is important to the understanding of our atmosphere.

Many aspects of these processes remain incompletely understood, however, including the oxidation of DMS.[5] For example, a recent work by James et al.[6] comparing measured and modeled results at a site in Mace Head, Ireland, show that the daytime oxidation rate of DMS is underestimated by models by over a factor of 3. Nighttime oxidation of DMS is thought to be dominated by reaction with nitrate radical (NO_3).[7,8] In the daytime, DMS is thought to be oxidized by reaction with the hydroxyl radical (OH).[9,10] This reaction has a recommended[11] room-temperature rate constant of 5.0×10^{-12} cm^3 molecule^{-1} s^{-1}. Due to an absence of a known alternative, it is common for models to include only OH and NO_3 as oxidation sources for DMS.[6]

Field measurements[12] have been made of iodine oxide (IO) in the MBL, also at the Mace Head site. However, because of the small number of measurements made to this point and the fact that these measurements are close to the current detection limit of IO in the field, how representative these concentrations are for the entire MBL is unknown. The authors of ref 12 speculate that IO is ubiquitous in the MBL. The main source of IO is biogenic,[13,14] in the form of organic iodine compounds such as CH_2I_2. Emission of these compounds correlates with times of high biogenic activity.[15] These compounds are photochemically converted to active iodine by photolysis to produce the I atom[16] followed by reaction with ozone (O_3) to produce IO.[17] A large fraction of iodine is thought to be in its active form (i.e. IO and I), due to the fast rate of photolysis of HOI,[18,19] a major reservoir species for iodine. Less is known about iodine chemistry than the chemistry of the other natural halogen species, chlorine and bromine. A more comprehensive explanation of IO studies, with special attention given to the IO radical self-reaction, can be found a recent work by Bloss et al.[20]

At one time, it was thought that DMS oxidation by IO,[21,22]

$$\mathrm{IO} + \mathrm{DMS} \rightarrow \mathrm{I} + \mathrm{DMSO} \qquad (1)$$

is an important reaction in the atmosphere. The measured rate constant in those works was on the order of 10^{-11} cm^3 molecule^{-1} s^{-1}. Those measurements were found to be in error, and the current recommended value of this rate constant is 1.2×10^{-14} cm^3 molecule^{-1} s^{-1} at room temperature,[11] with the temperature dependency of this reaction remaining unknown. The major obstacles in the earlier studies of reaction 1 include the following: (1) the uncertainty of the absorbance cross section of IO radical; (2) the uncertainty of the rate constant for the self-reaction of IO radical; (3) wall loss of the IO radical. This recommended value is based on three measurements by Maguin et al.,[23] Barnes et al.,[24] and Knight and Crowley,[25] as well as an upper limit set by Daykin and Wine.[26] The former three studies were done at low pressures (2 Torr or lower), and the study by Daykin and Wine (at 40, 100, and 300 Torr) found no pressure dependence.

In this work, we examine the reaction of IO radicals with DMS using cavity ring-down spectroscopy (CRDS). This technique was employed in a previous study,[27] performed in this laboratory, of the reaction of Br atoms and BrO radicals with DMS. In that work, the reaction of BrO radicals with DMS was found to have a pressure dependence. In this work, both the pressure and the temperature effects of reaction 1 are examined. In the process, we examine the high-resolution spectrum of the IO radical using laser spectroscopy. The low detection limit achieved by using the CRDS technique allows us to spectroscopicly observe IO radical directly and in a quantitative manner.

* To whom correspondence should be addressed. E-mail: kawasaki@photon.mbox.media.kyoto-u.ac.jp. Fax: +81-75-753-5526.

† Present address: California State University at Channel Islands, One University Drive, Camarillo, CA 93010.

10.1021/jp0345147 CCC: $25.00
Published on Web 07/26/2003

2. Experimental Section

The CRDS apparatus used in this study is described in detail elsewhere.[28] The system employs two pulsed lasers, a probe laser and a photolysis laser. The probe beam was generated by the 355 nm output of a Nd^{3+}:YAG laser (Spectra-Physics PRO-230). The beam was directed to an optical parametric oscillator (Spectra-Physics Quanta Ray MOPO-SL), with a tunable output range from 440 to 1800 nm. In this experiment, the idler output from the MOPO was then frequency doubled with a BBO crystal (Spectra-Physics FD-900) to obtain the desired wavelength range. This beam was used to probe the concentrations of reactive species in the system. After the photolysis laser beam traversed the cell nearly collinear to the axis of the ring-down cavity, the probe laser beam was injected through one of two high-reflectivity mirrors, which made up the ring-down cavity. The mirrors (Research Electronic Optics) had a specified maximum reflectivity of >0.9994 at 435 nm, a diameter of 7.8 mm, and a radius of curvature of 1 m and were mounted 1.04 m apart. Light leaking from one of the mirrors of the ring-down cavity was detected by a photomultiplier tube (Hamamatsu: R212UH) through a narrow band-pass filter for 442 nm. The decay of the light intensity was recorded using a digital oscilloscope (Tektronix TDS714L) and transferred to a personal computer. The decay of the light intensity is given by eq I,

Where I_0 and $I(t)$ are the intensities of light at time 0 and t, respectively. τ_0 is the empty cavity ring-down time (1.5 μs at 435.51 nm). L_R is the length of the reaction region (0.46 m). L is the cavity length (1.04 m). τ is the measured cavity ring-down time. n and σ are the concentration and absorption cross section of the species of interest, and c is the velocity of light.

$$I(t) = I_0 \exp(-t/\tau) = I_0 \exp(-t/\tau_0 - \sigma nc(L_R/L)t) \quad \text{(I)}$$

The reaction cell consisted of a Pyrex glass tube (21 mm i.d.) that was evacuated by a combination of an oil rotary pump and a mechanical booster pump. The temperature of the gas flow region was controlled by circulation of a thermostated mixture of ethylene glycol and water and was controllable over the range 273−312 K. The difference between the temperature of sample gas at the entrance and exit of the flow region was <1 K. The pressure in the cell was monitored by an absolute pressure gauge (Baratron). Gas flows were measured and regulated by mass flow controllers (KOFLOC: 3660). A slow flow of nitrogen gas was introduced at both ends of the ring-down cavity close to the mirrors to minimize deterioration caused by exposure to reactants and products. The total flow rate was about 2×10^3 cm^3 min^{-1} (STP).

Ozone was produced by irradiating the oxygen gas flow with the 184.6 nm output of a low-pressure Hg lamp (Hamamatsu L937) at high pressure (>720 Torr). It was measured upstream of the reaction tube by monitoring the absorption at 253.7 nm ($\sigma = 1.15 \times 10^{-17}$ cm^2)[11] using a separate low pressure Hg lamp as the light source. The probe lamp is covered with Vicol glass so that ozone is only detected and not generated from that light source. Typical ozone number densities of 4×10^{12} molecules cm^{-3} were generated in this way.

The 266 nm output of a Nd^{3+}:YAG laser (Spectra Physics GCR-250) was used to photodissociate ozone ($\sigma = 9.7 \times 10^{-18}$ cm^2) to give $O(^1D)$ atoms. The contribution of I atoms from the photodissociation of CF_3I at 266 nm is relatively minor, due to its small cross section ($\sigma = 6.8 \times 10^{-19}$ cm^2). The $O(^1D)$ atoms are relaxed by N_2 collisions to produce $O(^3P)$ atoms. IO radicals were formed by allowing $O(^3P)$ to react with CF_3I giving the following reaction sequence:

$$O_3 + h\nu\ (\lambda = 266\ \text{nm}) \rightarrow O(^1D) + O_2 \quad (2)$$

$$O(^1D) + N_2 \rightarrow O(^3P) + N_2 \quad (3)$$

$$O(^3P) + CF_3I \rightarrow IO + CF_3 \quad (4)$$

The rate constant for reaction 3 is 2.6×10^{-11} molecule^{-1} cm^3 s^{-1} at room temperature,[11] resulting in a lifetime of less than 0.2 μs for all experimental conditions in this study. The rate constant for reaction 4 was monitored using our system, with the results being presented in this work. The CF_3I concentration was varied as $(3-18) \times 10^{14}$ molecule cm^{-3} for determination of the rate constant of reaction 4. For determination of the rate constant of reaction 1, the CF_3I concentration was 8×10^{14} molecules cm^{-3}. The maximum IO radical concentrations (6×10^{11} molecules cm^{-3}) was observed to occur between 400 and 800 μs after the initial photolysis laser pulse. We also attempted the experiment using CH_3I instead of CF_3I but found that the yield of IO atoms was less. This is in agreement with previous work by Gilles et al.[29] That work demonstrated that the branching ratio of IO production from the $O(^3P)$ reaction with CH_3I was less than that of CF_3I by a factor of about 2 to 1. The IO radical concentration was monitored at 435.60 nm, corresponding to the $A^2\Pi_{3/2} \leftarrow X^2\Pi_{3/2}$ (3,0) band head. We measured the IO absorption cross section to be 5.9×10^{-17} cm^2 molecule^{-1} at this wavelength with a resolution of about 0.2 cm^{-1}. The IO concentration profile was measured between 800 and 10800 μs after the initial photolysis laser pulse. The decay profile was a result of the self-reaction of IO, as well as the reaction of IO with DMS.

Dimethyl sulfide (DMS, 98%) was purified using the freeze−pump−thaw method. DMS vapor was collected in an evacuated glass gas bulb. The bulb was then filled with N_2 to produce a 5% mixture of DMS/N_2. The amount of DMS in the reaction chamber was determined by using a mass flow controller. DMS number densities were varied between 5×10^{14} and 5×10^{15} molecules cm^{-3}. The other commercially obtained reagents, CF_3I (97%, Lancaster), N_2 (>99.999%), and O_2 (> 99.995%), were used without further purification.

3. Results

In the course of determining the rate constant for the reaction of IO with DMS, we measured the cross section of IO in the $A^2\Pi_{3/2} \leftarrow X^2\Pi_{3/2}$ (3,0) band head. We calculated the cross section at this wavelength by plotting the absorbance at this band against the known IO number density. This plot is shown in Figure 1. We determined the number density of IO by measuring the absorbance at 427.2 nm, the band head of the $A^2\Pi_{3/2} \leftarrow X^2\Pi_{3/2}$ (4,0) band. The cross section at this point is known from previous work by Harwood et al.,[30] 3.6×10^{-17} cm^2. The maximum absorbance for the $A^2\Pi_{3/2} \leftarrow X^2\Pi_{3/2}$ (3,0) band is at 435.60 nm, with a cross section of 5.9×10^{-17} cm^2. This is the first measured cross section of this band using laser spectroscopy with resolution of 0.2 cm^{-1}. As can be seen in Figure 1, the (3,0) band is a relatively structured band compared to the (4,0) band as reported by Harwood et al.[30] For this reason, when using a higher resolutions the (3,0) band head has a higher absorption cross section than the (4,0) band, in contrast to what has been reported.

Details of production of the IO are in the Experimental Section. IO was formed by reacting CF_3I with $O(^3P)$. We used the rise time of IO production to determine the rate constant

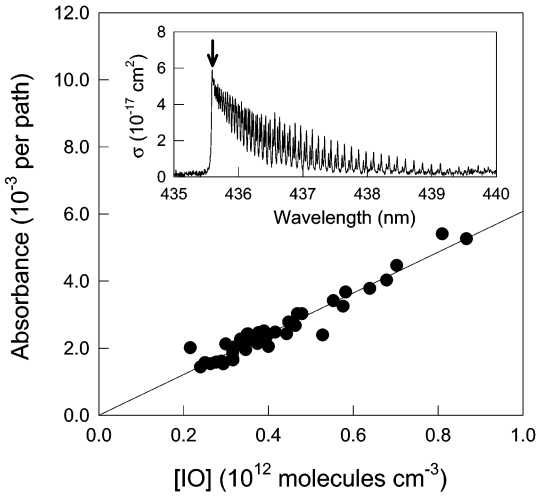

Figure 1. Absorbance of IO at the $A^2\Pi_{3/2} \leftarrow X^2\Pi_{3/2}$ (3,0) band head plotted against the concentration of IO. The $A^2\Pi_{3/2} \leftarrow X^2\Pi_{3/2}$ (3,0) band of IO is shown in the inlay box. An arrow marks the peak wavelength used in monitoring IO concentration.

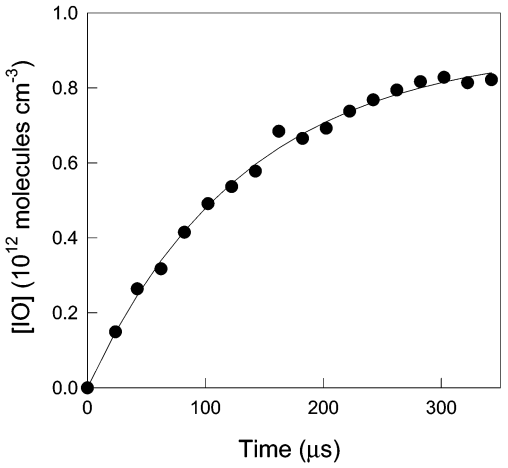

Figure 2. Rise profile of IO after the initial photolysis pulse (time = 0 μs) by 266 nm output of a Nd^{3+}:YAG laser.

for reaction 4. The rise time is shown in detail in Figure 2. From these data, we determined the rate constant for reaction 4 to be $(7.8 \pm 0.3) \times 10^{-12}$ molecule^{-1} cm^3 s^{-1} at room temperature. This vale is larger than some recently reported values by Gilles et al.[29] and by Holscher et al.[31] However, complications from the reaction of photolysis of the CF_3I were minimal in our system. This is because the reaction of $I + O_3$ is a relatively slow reaction (1.2×10^{-12} molecule^{-1} cm^3 s^{-1} at room temperature).[11] Also, as previously mentioned CF_3I has a relatively small cross section. Under experimental conditions, IO production from $I + O_3$ is estimated to be below 2% of the total contribution. CF_3 mostly reacts with O_2 to generate CF_3O_2, which is considered to be less reactive radical. Therefore, the contribution of the CF_3 reactions can be negligible. The effects of the reaction of O (^{3}P) with I_2 and IO are negligible, because these concentrations are much lower compared with CF_3I.

We then measured the IO concentration decay as a function of time. The IO is depleted due to the self-reaction,

$$IO + IO \rightarrow \text{products} \qquad (5)$$

and the IO reaction with DMS (reaction 1), as well as diffusion out of the detection region. Hence, the decay of IO can be analyzed as a sum of the first and second-order kinetics, and

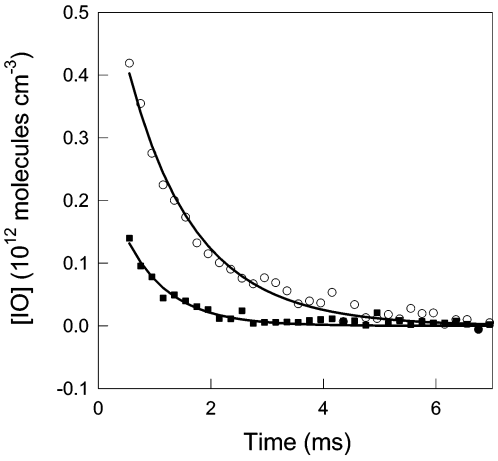

Figure 3. Decay profile of IO in the absence (open circles) and presence (filled squares) of DMS (1.6×10^{15} molecules cm^{-3}). Curves were fit to eq II. Data were taken at 100 Torr of N_2 diluent and 298 K.

the concentration of IO can be given by the following equation:

$$\frac{1}{[IO]_t} = \left\{\left(\frac{1}{[IO]_0} + \frac{2k_5}{k_1^{1st}}\right)\exp(k_1^{1st}t) - \left(\frac{2k_5}{k_1^{1st}}\right)\right\} \qquad (II)$$

Here $[IO]_t$ is the concentration of IO, $[IO]_0$ is the initial concentration of IO, k_5 is the rate constant of reaction 5, and t is the time. The self-reaction of IO shows no pressure or significant temperature dependencies under the range of conditions of this study.[30] The first-order term, k_1^{1st}, is the sum of the pseudo-first-order reaction of IO + DMS, plus loss due to diffusion.

$$k_1^{1st} = k_1[DMS] + k_d \qquad (III)$$

In the absence of DMS, IO removal is regulated by reaction 5 and by the diffusion rate. Figure 3 shows the decay profile of IO in our system in the absence of DMS. When we fit these data to eq II, we were able to calculate k_5 to be $(9.4 \pm 1.8) \times 10^{-11}$ molecule^{-1} cm^3 s^{-1} at room temperature. This is in reasonably good agreement with the NASA recommended[11] value of 8×10^{-11}. It is in excellent agreement with the value obtained by Harwood et al.,[30] 9.9×10^{-11} molecule^{-1} cm^3 s^{-1}.

We performed experiments to determine the rate constant for the reaction of IO with DMS, reaction 1. In addition to the plot with no DMS, Figure 3 also shows the decay profile of IO concentration with a DMS concentration of 1.6×10^{15} molecule cm^{-3}. Due to competition for O(^{3}P) with DMS, the maximum IO number densities decreases when the amount of DMS is increased. The reaction of O(^{3}P) with DMS affects to the only the initial concentration of IO; hence, there is no influence of this reaction for the determination of k_1^{1st}. DMS number densities ranged from 5×10^{14} to 5×10^{15} molecules cm^{-3}. We plot k_1^{1st} versus the DMS number density and fit the data using a linear regression. An example of this is shown in Figure 4. From this fit, we can obtain the rate constant for the IO + DMS reaction, k_1. At 5 Torr total pressure and room temperature, we calculate k_1 to be $(1.0 \pm 0.3) \times 10^{-14}$ molecule^{-1} cm^3 s^{-1}. This value corresponding to the NASA recommendation value,[11] 1.2×10^{-14} molecule^{-1} cm^3 s^{-1}, is based on the previous low-pressure studies[23-25] (<2 Torr), as well as the upper limit determined by Daykin and Wine.[26] As we increased the total pressure of the reaction chamber, we observed an increase in the rate constant. This pressure dependency was observed up to about 100 Torr total pressure, where the reaction seems to

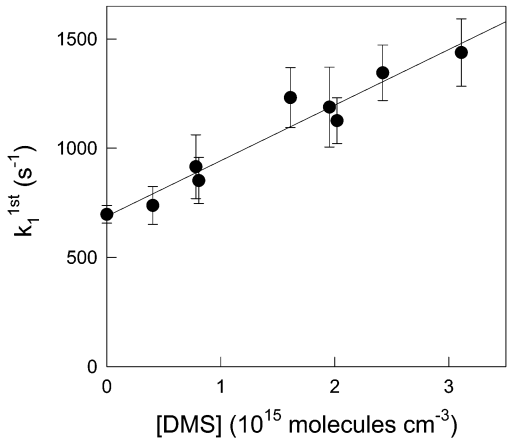

Figure 4. Second-order plot for the reaction of IO radicals with DMS in 100 Torr of N_2 diluent at 298 K. The line is a linear least-squares fit.

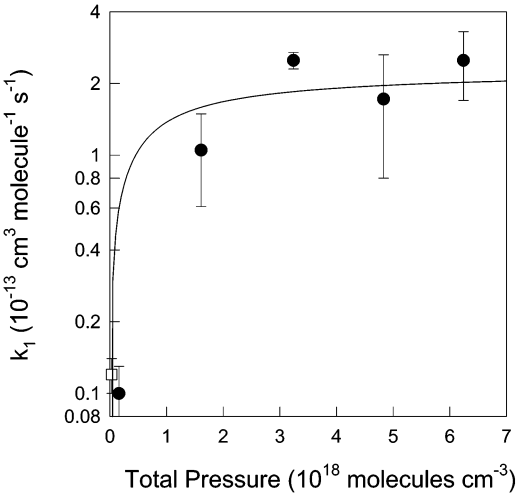

Figure 5. Rate constant of IO radicals with DMS as a function of N_2 diluent pressure at 298 K. The plot includes the NASA/JPL recommended value (open square) at 1 Torr total pressure.[11]

TABLE 1: Rate Constant of IO + DMS at 298 K with Several Pressures of N_2 Diluent

tot. pressure (Torr of N_2)	$10^{14}k_1$ (molecule^{-1} cm^3 s^{-1})	tot. pressure (Torr of N_2)	$10^{14}k_1$ (molecule^{-1} cm^3 s^{-1})
5	1.0 ± 0.3	150	17 ± 9
50	11 ± 4	200	25 ± 8
100	25 ± 2		

reach a high-pressure limit. At 100 Torr, our measured rate constant is $(2.5 \pm 0.2) \times 10^{-13}$ molecule^{-1} cm^3 s^{-1}, while at 200 Torr total pressure our measured rate constant is $(2.5 \pm 0.8) \times 10^{-13}$ molecule^{-1} cm^3 s^{-1}. The observed rate constants at room temperature, with varying pressures from 5 to 200 Torr, are listed in Table 1. The NASA recommended value previously measured is also included in Figure 5. These data have been used to fit the pressure dependence of the rate constant to the following empirically derived equation:

$$k_1 = \left(\frac{k_1^{low}[M]}{1 + (k_1^{low}[M]/k_1^{high})}\right) \times 0.6^{\{1+[\log(k_1^{low}[M]/k_1^{high})]^2\}^{-1}} \quad \text{(IV)}$$

In this equation, k_1 is the observed rate constant for reaction 1, k_1^{low} and k_1^{high} are the low and high pressure limits, and $[M]$ is the total number density. The rate constants, including the best-fit curve, are plotted versus total pressure in Figure 5. It is worth

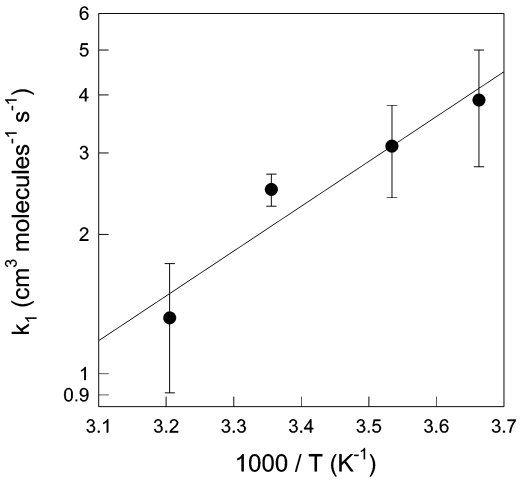

Figure 6. Arrhenius plot for the reaction of IO radicals with DMS. Data were taken at 100 Torr of N_2 diluent.

TABLE 2: Rate Constant of IO + DMS with 100 Torr of N_2 Diluent at Several Temperatures

temp (K)	$10^{13}k_1$ (molecule^{-1} cm^3 s^{-1})	temp (K)	$10^{13}k_1$ (molecule^{-1} cm^3 s^{-1})
273	3.9 ± 1.1	298	2.5 ± 0.2
283	3.1 ± 0.7	312	1.3 ± 0.4

noting that, as recently shown by Troe,[32] the value of 0.6 in the equation above is an empirically derived parameter. In actuality, the value can vary by a factor of 2 or more. In the case of our data, the above equation fit the results reasonably, but other values of that parameter ranging from 0.3 to 0.8 also fit the equation within error limits. The value for k_1^{high} was determined to be $(2.5 \pm 0.2) \times 10^{-13}$ molecule^{-1} cm^3 s^{-1}. The low-pressure rate constant, k_1^{low}, determined from the fit to the equation above, is $(8.9 \pm 5.2) \times 10^{-31}$ molecule^{-2} cm^6 s^{-1}.

The pressure dependence observed in this work is in direct contrast to the previous study of Daykin and Wine.[26] In that work, the authors performed experiments at 40, 100, and 300 Torr total pressure. In those experiments, the photolysis of NO_2 produced oxygen atoms, which reacted with I_2 to produce IO. Another major difference between that work and ours is that the DMS concentration was 1−2 orders of magnitude larger in the study of Daykin and Wine, while the IO concentration is about twice as large in their work.

We also measured the temperature dependence of reaction 1. The values of the rate constant at various temperatures from 273 to 312 K are listed in Table 2. From these data, we constructed an Arrhenius plot shown in Figure 6. Linear least-squaresd analyses of the data in Figure 6 yield the following expression:

$$k_1 = 1.2^{+4.5}_{-1.0} \times 10^{-16} \times \exp[(2230 \pm 460)/T] \text{ molecule}^{-1} \text{ cm}^3 \text{ s}^{-1} \quad \text{(V)}$$

We believe this is the first determination of the Arrhenius expression for the reaction of IO with DMS. This reaction exhibits a negative activation energy of -18.5 ± 3.8 kJ mol^{-1}. This is consistent with what was observed in the reaction of BrO with DMS. As in that reaction, it suggests a mechanism involving a complex intermediate species:

$$\text{IO} + \text{DMS} \rightleftarrows [\text{IO-DMS}] \rightarrow \text{I} + \text{DMSO} \quad \text{(1a)}$$

The magnitude of the negative activation energy suggests a longer lived intermediate than is the case for BrO−DMS. This

is consistent with the larger pressure effects seen for this reaction. The large pressure effect of this reaction is evidence for the termolecular reaction path. This effect is greater for IO + DMS than for BrO + DMS. A recent study by Williams et al.[33] shows that the adduct of OH with DMS may be underestimated at lower temperatures. On the basis of these studies, DMS seems to readily form adducts with potential oxidizers.

The relative reactivity of halogen oxides (XO) toward DMS at pressures relevant to the atmosphere follows the pattern BrO $\approx$ IO > ClO. This is in contrast to a previously reported study based on low-pressure studies, which claims that the reactivities of IO and ClO are similar. All reactions of these halogen oxides with DMS are thought to produce DMSO. As previously[34] pointed out, on the basis of thermodynamic arguments, it might be expected the order of reactivity is IO > BrO $\gg$ ClO. Our calculated change in enthalpy uses data taken from ref 11. The change in enthalpy of these reactions is listed below.

$$\mathrm{IO + DMS \rightarrow I + DMSO} \qquad \Delta H_f(298) = -134\ \mathrm{kJ\ mol^{-1}} \quad (1)$$

$$\mathrm{BrO + DMS \rightarrow Br + DMSO} \qquad \Delta H_f(298) = -127\ \mathrm{kJ\ mol^{-1}} \quad (6)$$

$$\mathrm{ClO + DMS \rightarrow Cl + DMSO} \qquad \Delta H_f(298) = -94.5\ \mathrm{kJ\ mol^{-1}} \quad (7)$$

The exothermicity of these reactions seems to agree with our observed reactivity order for XO + DMS. This thermodynamic argument is based primarily on the difference in bond dissociation energy of the halogen oxide. It is worth noting that, for BrO and IO, this value has an uncertainty of about 10%. There is also uncertainty related to the measured rate constants. These errors combined may improve the reaction enthalpy correlation to the reaction kinetics.

The difference in reactivity between IO and BrO may also be attributed to steric hindrance. IO may have a lower probability, with respect to BrO, to be properly oriented for reaction. There is evidence for this in the apparently much smaller preexponential factor observed for the IO + DMS reaction than for the BrO + DMS reaction. This would be expected given the size of iodine with respect to bromine. This argument cannot be extended to the ClO case, for which the preexponential factor has been recently measured[35] to be smaller than that for BrO.

Ionic curve-crossing models[36] provide an alternative explanation of these relative reactivities to the ones presented above. In that model, relative reactivities of radical−molecule reactions can be accurately predicted on the basis of the thermodynamics of the ionic potential energy surface. This model is noted[37] for its ability to explain the reactivity of OH and chlorine atom (Cl) reactions with a series of alkanes. In that case, the increase in the rate constant for a particular electron acceptor, the radical, is associated with the ionization energy of the electron donor, the alkane. In the case of XO + DMS, the halogen oxide is the electron acceptor; hence, its reactivity in this type of reaction should be associated with its electron affinity. The electron affinities for IO, BrO, and ClO are 2.38, 2.35, and 2.38 eV,[38] respectively. Again, the trend seen in the bond dissociation model is followed. It is not entirely clear to these authors whether a difference in these values, about 10 kJ mol^{-1}, can cause such a dramatic difference in the reaction rates.

In light of the data presented in this work, it does seem that the reaction mechanisms of IO + DMS and BrO + DMS involve a complex intermediate. Indeed, Diaz-de-Mera et al.[35] postulate such a mechanism for the reaction of ClO + DMS in their recent work. We expect that the stability of the intermediate is greater in the case of IO and BrO than for ClO. The greater stability translates to a longer lifetime to allow the reaction to proceed to form DMSO + X:

$$\mathrm{XO + DMS \rightleftarrows [XO{-}DMS]^{\ddagger} \xrightarrow{+M} [XO{-}DMS] \rightarrow X + DMSO} \quad \text{(VI)}$$

This interpretation of the results is speculative, however, and clearly more detailed studies of the reaction mechanism are needed to fully explain the reaction trend.

4. Atmospheric Implications

DMS is ubiquitously emitted from the oceans of the world from biological sources.[39] It is the most important source of sulfur from the oceans.[39] Average mixing ratios in the marine boundary layer are around 100 ppt,[39] but concentrations are highly variable with biological and tidal activity, as well as climate. Oxidation of DMS eventually produces highly water-soluble species with low vapor pressures, such as sulfuric (H_2SO_4) and methanesulfonic acid (CH_3SO_2OH, MSA).[1] These species are thought to form the building blocks of aerosol production for a large number of atmospheric particles,[40,41] hence the link between oxidation of DMS and aerosol formation. DMS is removed less efficiently at night, when oxidation is dominated by nitrate radical (NO_3).[42,43]

A predominate sink of DMS during the day is reaction with OH.[9,10] Oxidation of DMS is far from completely understood.[6,44] As mentioned earlier in this work, one study[6] showed that oxidation of DMS by OH was underestimated by a factor of 3 in the MBL at the Mace Head site. The rate constant[11] for this reaction of OH with DMS is 5.0×10^{-12} cm^3 molecule^{-1} s^{-1} at room temperature, with some large uncertainty in this value at lower temperatures. A recent work[33] finds that this rate constant is underestimated at much lower temperatures, but it is unlikely that this can be used to explain the discrepancy.

The lack of understanding of DMS oxidation has led to a search for other sinks, such as chlorine atom. Recently, measurements[45] have indicated the amount of molecular chlorine in the marine boundary layer is much larger than previously thought. Chlorine atom reacts rapidly with DMS, with a rate constant of about 3.3×10^{-10} cm^3 molecule^{-1} s^{-1} at room temperature.[46] The modeling work by James et al.[6] suggests that DMS oxidation by Cl cannot account for the measurement results observed because peak concentrations are too short-lived. It has been shown[43] that the Cl + DMS reaction can proceed via an adduct, as well as via hydrogen abstraction. The hydrogen abstraction path leads to the formation of aerosols, while the fate of the adduct is unclear.[1] There is some evidence[47] that the Cl−DMS adduct can react with oxygen to produce DMSO, but further studies are needed.

Reaction of DMS with halogen oxide molecules has been speculated to play a role in the atmosphere for some time.[21,39] Reaction with ClO and BrO (as well as IO) has been deemed too slow to compete with OH and Cl oxidation.[1] This is due to a slow rate constants for DMS with ClO (9.5×10^{-15} cm^3 molecule^{-1} s^{-1} at 300 K) and with BrO (4.2×10^{-13} cm^3 molecule^{-1} s^{-1} at 300 K).[24,27,35] Maximum BrO number densities in the MBL are thought to be on the order of 1×10^7 molecules cm^{-3}.[48] Arctic air can contain larger amounts of halogen oxides,[49] but this is not considered typical of the MBL.

It is not known to the authors how mixing of this air can effect DMS oxidation in the MBL in places such as the Mace Head site.

Recent measurements show that concentrations of iodine monoxide (IO) in the marine boundary layer are much higher than previously thought.[14] These data show marine boundary layer IO seems to be predominately produced by the photolysis and oxidation of CH_2I_2. While CH_3I is the most abundant iodine-containing species emitted from the oceans, CH_2I_2 is photolyzed by longer wavelength light,[16] hence acting as the source of IO in the lower atmosphere more efficiently. There is further evidence of this in the work of Simpson et al.,[50] showing that CH_3I and DMS concentrations are not correlated in the MBL. Measurements by Carpenter et al.[14] show that IO concentrations can reach as high as 1.5×10^8 molecules cm^{-3}. It should be noted that there are only a few measurements of IO in the MBL and more measurements need to be made to assess its significance. The room-temperature rate constant measured in this work is 2.5×10^{-13} cm^3 $molecule^{-1}$ s^{-1}. Under these conditions, the lifetime of DMS with respect to IO is about 7.4 h. It should be noted that, for the field measurements,[14] IO concentrations were below the detection limit of the instrumentation on most days. The detection limits for the quoted measurements are near 5×10^7 molecules cm^{-3}. However, even using the detection limit as a typical maximum of IO, the lifetime of DMS with respect to IO becomes 22 h. The daily temporal profile of IO concentration should generally be similar to that of OH because they are both produced by photolysis of species (O_3 and CH_2I_2) that absorb light in roughly the same region of the solar spectrum. Furthermore, recent works by de Chen et al.[51] show an underestimation of DMSO yield from DMS oxidation. Oxidation by halogen oxides is thought to produce DMSO with a yield of almost unity.[1]

5. Conclusions

We have measured the pressure and temperature dependencies of the reaction of IO + DMS. The rate constant was measured by using cavity ring-down spectroscopy. This allowed us to measure a small amount of IO, reducing the uncertainties associated with some other techniques, such as wall loss. At lower pressures, the rate constant was found to be in reasonable agreement with previously reported values. The reaction shows a pressure dependence, however. Under atmospheric conditions relevant to the marine boundary layer, we show that IO can be an important oxidizer of DMS. For this reason, modeling studies and field measurement campaigns should be performed to provide better understanding of this critical topic.

Acknowledgment. This work is supported by a Grant-in-Aid for the priority research field "Radical Reactions" from the Ministry of Education of Japan. S.A. thanks the Japan Society for Promotion of Science for a fellowship.

References and Notes

(1) Finlayson-Pitts, B. J.; Pitts, J. N. *Chemistry of the Upper and Lower Atmosphere*; Academic Press: San Diego, CA, 1999.

(2) Aneja, V. P. *J. Air Waste Manage. Assoc.* **1990**, *40*, 469−476.

(3) Charlson, R. J.; Lovelock, J. E.; Andreae, M. O.; Warren, S. G. *Nature* **1987**, *326*, 655−661.

(4) Houghton, J. T.; Ding, Y.; Griggs, D. J.; Noguer, M.; van der Linden, P. J.; Xiaosu, D.; Maskell, K.; Johnson, C. A. *Climate Change 2001: The Scientific Basis*; Contribution of Working Group I to the Third Assessment Report of the Intergovernmental Panel on Climate Change (IPCC); Cambridge University Press: New York, 2001 (ISBN: 05210 14956 2001).

(5) Ravishankara, A. R.; Rudich, Y.; Talukdar, R.; Barone, S. B. *Philos. Trans. R. Soc. London, Ser. B* **1997**, *352*, 171−181.

(6) James, J. D.; Harrison, R. M.; Savage, N. H.; Allen, A. G.; Grenfell, J. L.; Allan, B. J.; Plane, J. M. C.; Hewitt, C. N.; Davison, B.; Robertson, L. *J. Geophys. Res.* **2000**, *105*, 26379−26392.

(7) Wallington, T. J.; Atkinson, R.; Winer, A. M.; Pitts, J. N. *J. Phys. Chem.* **1986**, *90*, 4640−4644.

(8) Dlugokencky, E. J.; Howard, C. J. *J. Phys. Chem.* **1988**, *92*, 1188−1193.

(9) Hynes, A. J.; Wine, P. H.; Semmes, D. H. *J. Phys. Chem.* **1986**, *90*, 4148−4156.

(10) Barone, S. B.; Turnipseed, A. A.; Ravishankara, A. R. *J. Phys. Chem.* **1996**, *100*, 14694−14702.

(11) DeMore, W. B.; Sander, S. P.; Golden, D. M.; Hampson, R. F.; Kurylo, M. J.; Howard, C. J.; Ravishankara, A. R.; Kolb, C. E.; Molina, M. J. *Chemical Kinetics and Photochemical Data for use in Stratospheric Modeling, JPL Publication 97-4*; Jet Propulsion Laboratory: Pasadena, CA, 1997.

(12) Alicke, B.; Habestreit, K.; Stutz, J.; Platt, U. *Nature* **1999**, *397*, 572−573.

(13) Happell, J. D.; Wallace, D. W. R. *Geophys. Res. Lett.* **1996**, *23*, 2105−2108.

(14) Carpenter, L. J.; Sturges, W. T.; Penkett, S. A.; Liss, P. S.; Alicke, B.; Hebestreit, K.; Platt, U. *J. Geophys. Res.* **1999**, *104*, 1679−1689.

(15) Yokouchi, Y.; Nojiri, Y.; Barrie, L. A.; Toom-Sauntry, D.; Fujinuma, Y. *J. Geophys. Res.* **2001**, *106*, 12661−12668.

(16) Roehl, C. M.; Burkholder, J. B.; Moortgat, G. K.; Ravishankara, A. R.; Crutzen, P. J. *J. Geophys. Res.* **1997**, *102*, 12819−12829.

(17) Turnipseed, A. A.; Giles, M. K.; Burkholder, J. B.; Ravishankara, A. R. *Chem. Phys. Lett.* **1995**, *242*, 427−434.

(18) Bauer, D.; Ingham, T.; Carl, S. A.; Moortgat, G. K,; Crowley, J. N. *J. Phys. Chem. A* **1998**, *102*, 2857−2864.

(19) Rowley, D. M.; Mossinger, J. C.; Cox, R. A.; Jones, R. L. *J. Atmos. Chem.* **1999**, *34*, 137−151.

(20) Bloss, W. J.; Rowley, D. M.; Cox, R. A.; Jones, R. L. *J. Phys. Chem. A* **2001**, *105*, 7840−7854.

(21) Martin, D.; Jourdain, J. L.; Laverdet, G.; Le Bras, G. *Int. J. Chem. Kinet.* **1987**, *19*, 503−512.

(22) Barnes I.; Becker, K. H.; Carlier, P.; Mouvier, G. *Int. J. Chem. Kinet.* **1987**, *19*, 489−501.

(23) Maguin, F.; Mellouki, A.; Laverdet G.; Poulet, G.; Le Bras, G. *Int. J. Chem. Kinet.* **1991**, *23*, 237−245.

(24) Barnes, I.; Bastian, V.; Becker, K. H.; Oerath, R. D. *Int. J. Chem. Kinet.* **1991**, *23*, 579−591.

(25) Daykin, E. P.; Wine, P. H. *J. Geophys. Res.* **1990**, *95*, 18547−18553.

(26) Knight, G. P.; Crowley, J. N. *Phys. Chem. Chem. Phys.* **2001**, *3*, 393−401.

(27) Nakano, Y.; Goto, M.; Hashimoto, S.; Kawasaki, M.; Wallington, T. J. *J. Phys. Chem. A* **2001**, *105*, 11045−11050.

(28) Ninomiya, Y.; Hashimoto, S.; Kawasaki, M.; Wallington, T. J. *Int. J. Chem. Kinet.* **2000**, *32*, 125−130.

(29) Gilles, M. K.; Turnipseed, A. A.; Talukdar, R. K.; Rudich, Y.; Villalta, P. W.; Huey, L. G.; Burkholder, J. B.; Ravishankara, A. R. *J. Phys. Chem.* **1996**, *100*, 14005−14015.

(30) Harwood, M. H.; Burkholder, J. B.; Hunter, M.; Fox, R. W.; Ravishankara, A. R. *J. Phys. Chem. A* **1997**, *101*, 853−863.

(31) Holscher, D.; Fockenberg, C.; Zellner, R. *Ber. Bunsen-Ges. Phys. Chem.* **1998**, *102*, 716−722.

(32) Troe, J. *Int. J. Chem. Kinet.* **2001**, *33*, 878−889.

(33) Williams, M. B.; Campuzano-Jost, P.; Bauer, D.; Hynes, A. J. *Chem. Phys. Lett.* **2001**, *344*, 61−67.

(34) Barnes, I.; Bastian, V.; Becker, K. H.; Overath, R. D. *Int. J. Chem. Kinet.* **1991**, *23*, 579−591.

(35) Diaz-de-Mera, Y.; Aranda, A.; Rodriguez, D.; Lopez, R.; Cabanas, B.; Martinez, E. *J. Phys. Chem. A* **2002**, *106*, 8627−8633.

(36) Donahue, N. M. *J. Phys. Chem. A* **2001**, *105*, 1489−1497.

(37) Smith, I. W. M.; Ravishankara, A. R. *J. Phys. Chem. A* **2002**, *106*, 4798−4807.

(38) Gilles, M. K.; Polak, M. L.; Lineberger, W. C. *J. Chem. Phys.* **1992**, *96*, 8012−8020.

(39) Seinfeld, J. H.; Pandis, S. N. *Atmospheric Chemistry and Physics*; John Wiley and Sons: New York, 1998.

(40) Charlson, R. J.; Lovelock, J. E.; Andreae, M. O.; Warren, S. G. *Nature* **1987**, *326*, 655−661.

(41) Andreae, M. O.; Crutzen, P. J. *Science* **1997**, *276*, 1052−1058.

(42) Wallington, T. J.; Atkinson, R.; Winer, A. M.; Pitts, J. N., Jr. *J. Phys. Chem.* **1986**, *90*, 5293−5396.

(43) Butkovskaya, N. I.; Le Bras, G. *J. Phys. Chem.* **1994**, *98*, 2582−2591.

(44) de Bruyn, W. J.; Harvey, M.; Cainey, J. M.; Saltzman, E. S. *J. Atmos. Chem.* **2002**, *41*, 189−209.
(45) Spicer, C. W.; Chapman, E. G.; Finlayson-Pitts, B. J.; Plastridge, R. A.; Hubbe, J. M.; Fast, J. D.; Berkowitz, C. M. *Nature* **1998**, *394*, 353−356.
(46) Stickel, R. E.; Nicovich, J. M.; Wang, S.; Zhao, Z.; Wine, P. H. *J. Phys. Chem.* **1992**, *96*, 9875−9883.
(47) Kinnison, D. J.; Mengon, W.; Kerr, J. A. *J. Chem. Soc., Faraday Trans.* **1996**, *92*, 369−372.
(48) Grenfell, J. L.; Harrison, R. M.; Allen, A. G.; Shi, J. P.; Penkett, S. A.; O'Dowd, C. D.; Smith, M. H.; Hill, M. K.; Robertson, L.; Hewitt, C. N.; Davison, B.; Lewis, A. C.; Creasey, D. J.; Heard, D. E.; Hebestreit, K.; Alicke, B.; James, J. *J. Geophys. Res.* **1999**, *104*, 13771−13780.
(49) Tuckermann, M.; Ackermann, R.; Golz, C.; Lorenzen-Schmidt, H.; Senne, T.; Stutz, J.; Trost, B.; Unold, W.; Platt, U. *Tellus, Ser. B* **1997**, *49*, 533−555.
(50) Simpson, I. J.; Colman, J. J.; Swanson, A. L.; Bandy, A. R.; Thornton, D. C.; Blake, D. R.; Rowland, F. S. *J. Atmos. Chem.* **2001**, *39*, 191−213.
(51) Chen, G.; Davis, D. D.; Kasibhatla, D.; Bandy, A. R.; Thorton, D. C.; Hubert, B. J.; Clark, A. D.; Blomquist, B. W. *J. Atmos. Chem.* **2000**, *37*, 137−160.